

Multiscale Nonlinear Constitutive Modeling of Carbon Nanostructures Based on Interatomic Potentials

J. Ghanbari¹ and R. Naghdabadi^{1,2}

Abstract: Continuum-based modeling of nanostructures is an efficient and suitable method to study the behavior of these structures when the deformation can be considered homogeneous. This paper is concerned about multiscale nonlinear tensorial constitutive modeling of carbon nanostructures based on the interatomic potentials. The proposed constitutive model is a tensorial equation relating the second Piola-Kirchhoff stress tensor to Green-Lagrange strain tensor. For carbon nanotubes, some modifications are made on the planar representative volume element (RVE) to account for the curved atomic structure resulting a non-planar RVE. Using the proposed constitutive model, the elastic behavior of the graphene sheet and carbon nanotube are studied.

Keywords: Multiscale modeling, Continuum-based modeling, Constitutive modeling, Carbon nanotubes, Graphene sheet.

1 Introduction

Carbon nanostructures like nanotubes and graphene sheets have attracted researchers' interest because of their many interesting properties. A variety of methods have been developed to study the mechanical behavior of nanotubes [Belytschko and Xiao (2003), Arroyo and Belytschko (2002), Wagner and Liu (2003), Zhang et al. (2003)]. There are several methods such as ab initio, Molecular Dynamics (MD), and Monte Carlo methods to study the atomic scale deformation which can capture every non-homogeneous atomic level data [Arroyo and Belytschko (2002), Wagner and Liu (2003), Tadmor et al. (1999)]. The main shortcoming of these methods is the limitations on the length and time scales under study. When the atomic level accuracy is not the major concern, continuum mechanics can be applied to study the overall behavior (and not individual atomic level) of the structure.

¹ Department of Mechanical Engineering, Sharif University of Technology, P.O. Box: 11365-3567, Tehran, Iran

² Institute for Nano Science and Technology, Sharif University of Technology, Tehran, Iran

The methodology of the continuum mechanics is developed throughout more than a century and the numerical applications of the developed models have been strengthened in recent decades. In recent years, different authors have presented various methods concerning continuum-based method. Odegard and Gates (2002) have suggested using an intermediate truss model for the atomic structures to be equivalent to the continuum model. Using the method, they have studied and determined elastic constants such as Young's modulus of carbon nanotubes. Odegard et al. (2004) have recently proposed a constitutive model for cross-linked nanotubes by using energy equivalence and determined material constants. Arroyo and Belytschko (2002) have presented an atomistic based finite deformation membrane for single layer crystalline films and carbon nanotubes. In their formulation, they have employed a modified Born rule, the so-called exponential Born rule, to relate the undeformed and deformed bond vectors through the deformation gradient tensor. They have studied several deformation modes of carbon nanotubes and compared them with the atomic simulations.

Wagner and Liu (2003) have used the method of scale decomposition on the displacement field in their continuum formulation for the nanostructures. In their method, the concept of bridging scale has been introduced and employed to couple the atomistic data with continuum data. He et al. (2004) have used a continuum model for size-dependent deformation of elastic films of nano-scale thickness. They have introduced a length scale parameter in the plate formulation and have studied the effects of the length scale on the behavior of the nano-scale film. Zhang et al. (2002) have determined the elastic modulus of single wall carbon nanotubes using a continuum analysis incorporating interatomic potentials. Wu et al. (2006) have studied the elastic properties of nanotubes using an energy-equivalent model. Using micropolar mechanics, Xie and Long (2006) studied the vibrational behavior of carbon nanotubes. In another work, Xie et al. (2007) used a continuum model to study the vibrational behavior of multi-walled carbon nanotubes. In their semi-analytical model, a set of eigenvalue dynamical equations derived from the Hamilton's principle is solved and the normal modes are obtained. Chakrabarty and Cagin (2008) studied the mechanical and thermal properties of various nanotubes and carbon nanotube based nanostructures.

Behfar and Naghdabadi (2006) have studied nanoscale modeling of a multi-shell fullerene embedded in an elastic medium, deriving explicit equations for the motion of the multi-shell fullerene based on continuum shell theory. They have also studied the vibrational behavior of multi-shell fullerenes. Behfar and Naghdabadi (2005) have also investigated vibrational behavior of multi-layered graphene sheets based on the continuum plate formulation. Sohi and Naghdabadi (2007a) using a continuum-based multi-layer shell theory have studied torsional buckling of car-

bon nanopeapods, proposing an equivalent pressure distribution for van der Waals interactions between fullerenes and carbon nanotubes. In a recent work, Sohi and Naghdabadi (2007b) have investigated the stability of single-walled carbon nanopeapods under hydrostatic pressure using the continuum shell model and determined the critical hydrostatic pressure for structural instability.

Using an analytical and finite element method, Kalamkarov et al. (2006) investigated the variation of elastic properties of nanotubes with respect to tube diameter. Tserpes and Papanikos (2005) proposed a finite element model to study the behavior of carbon nanotubes. More exact ab-initio methods have also been used to study the properties of nanotubes. Peng et al. (2006) used an ab-initio software to study the effects of diameter on the mechanical and electronic properties of nanotube. Yu et al. (2004) studied shear modulus of nanotubes with MD simulations. Using tight-binding theories, Hernandez et al. (1999) studied elastic properties of single-walled nanotubes.

Multiscale approaches have also attracted researchers' interest in studying medium to large nanostructures with respect to MD limitations [Karakasidis and Charitidis (2006), Ghoneim et al. (2003), Horstemeyer et al. (2003), Deymier and Vasseur (2002), Weinman et al. (2003), Maiti (2006)]. Multiscale methods can be classified in two main categories: concurrent methods and hierarchical methods. In concurrent methods, the domain under study is explicitly divided into some subdomains in which different theories may govern the behavior of the structure [Li and Chou (2006), Qian et al. (2004), Lourie et al. (2005), Wuite and Adali (2005)]. As an example, in crack propagation problems, since the exact modeling of crack tip is very important in propagating crack, the subdomain that includes crack tip is usually modeled by an exact method such as MD, or even quantum mechanics method. The remaining part of the domain where the overall behavior of the material is needed, is usually modeled by intrinsically averaging methods such as finite element method. Data exchange is done in the common boundary of subdomains, the so called handshake region. Horstemeyer et al. (2003) analyzed simple shear deformation using a multiscale scheme. Deymier and Vasseur (2002) presented a concurrent multiscale method of an atomic crystal coupled with elastic continuum. Recently, Maiti (2006) studied multiscale methods and their application on modeling of carbon nanotubes. Li and Chou (2006) have studied compressive behavior of carbon nanotube/polymer composites using a molecular mechanics multiscale approach.

In hierarchical methods [Sheng et al. (2004), Hou and Wu (1997), Zbib and Rubia (2002), Gosh (2003), Li et al. (2004), Kaminsky (2005), Chung and Namburu (2003)], every scale is present in the whole domain. The smaller scale is solved first and then the larger scale is formulated using the smaller scale results. These

methods are suitable for problems in which the time or length scales are larger than the computational limitations of the more exact methods such as MD, and in problems in which the critical point is not known a priori. Sheng et al. (2004) using a micromechanical analysis, presented a multiscale approach to the analysis of polymer/clay nanocomposites. Hou and Wu (1997) presented a multiscale finite element method for the analysis of composite materials and porous media. Zbib and Rubia (2002) introduced a multiscale model for plasticity. Smaoui et al (2006) studied the behavior of nonlinear porous media based on a linear iterative homogenization scheme.

In this paper, we have proposed a multiscale nonlinear tensorial constitutive model for the analysis of carbon nanostructures using modified Morse potential. The constitutive model is presented in total Lagrangian description and is suitable for finite element implementation and studying large deformation problems. All the atomic data provided by the modified Morse potential is represented in the constitutive model without any simplification. For curved nanostructures like carbon nanotubes, the effects of the curvature and tube diameter is considered in the formulation with modifications on the bonds and bond angles. Using the presented constitutive model, tension and shear deformation of the graphene sheet and carbon nanotube have been studied and the Young's and shear modulus of nanotubes with various diameters are compared with those available in the literature.

2 Interatomic potential for carbon nanostructures

There are several interatomic potentials for carbon nanostructures such as Tersoff-Brenner [Brenner (1990)], Morse [Morse (1929)], and modified Morse [Belytschko et al. (2002)]. Considering an atomic structure of a carbon nanosystem, the Morse potential is written as:

$$E_r = D[e^{-\alpha(r-r_0)} - 1]^2 \quad (1)$$

where r_0 is the bond length of the atomic structure in the undeformed (relaxed) configuration and r is the corresponding length in the deformed configuration. Also, D and α are constants. The relationship between bond elongation and restoring force is expressed as:

$$F_r = \frac{dE_r}{dr} = \{-2\alpha D e^{-\alpha(r-r_0)} [e^{-\alpha(r-r_0)} - 1]\} \quad (2)$$

As bond elongation increases, the Morse potential energy becomes more accurate. The form of Morse potential energy originally derived empirically and later supported by quantum mechanics.

The interatomic bonds in nanotubes are hybridized sp^2 bonds. The modified Morse potential function in which a bond angle variation term is expressed as:

$$\begin{aligned} E &= E_{stretch} + E_{angle} \\ E_{stretch} &= D_e \{ [1 - e^{-\beta(r-r_0)}]^2 - 1 \} \\ E_{angle} &= \frac{1}{2} k_\theta (\theta - \theta_0)^2 [1 + k_{sextile} (\theta - \theta_0)^4] \end{aligned} \quad (3)$$

The constants are listed as follows:

$$\begin{aligned} r_0 &= 1.39 \times 10^{-10} m, \quad D_e = 6.03105 \times 10^{-19} N.m, \\ \beta &= 2.625 \times 10^{10} /m, \quad \theta_0 = 2.094 rad, \\ k_\theta &= 0.9 \times 10^{-18} N.m/rad^2, \quad k_{sextile} = 0.754 rad^{-4} \end{aligned} \quad (4)$$

It is noted that the elongation energy in the modified Morse potential differs from the Morse potential (Eq. 1) in just a shift in the energy reference point, thus, upon differentiating, the result for both will be the same.

3 Nanoscale continuum theory for carbon nanostructures

Linking the discrete atomic structure to a continuum notion is done by using two major assumptions; namely the Born-Oppenheimer assumption [Born and Oppenheimer (1927)] and the Cauchy-Born rule [Erickson (1984)]. The Born-Oppenheimer assumption is used to link the displacement fields in the two atomic and continuous media. It says that the displacements are equal in the two media wherever their concepts are defined, i.e. at the atomic nuclei positions. The displacements of the interior points in the continuous medium are obtained using a proper interpolation of the displacements of the nearer nuclei positions. The other assumption, the Cauchy-Born rule, links the deformation of the atomic bonds to the concepts defined in the continuum mechanics theory. This rule states that the deformed bond (direction and length like a vector) is related to the undeformed bond by the deformation gradient tensor. This assumption is an approximation to the continuum mechanics because the deformation gradient tensor maps the infinitesimal line elements in the undeformed to the corresponding infinitesimal line elements in the deformed configuration, thus, the application of this map to finite-length line elements (in this case the bond vector) involves approximation. The Cauchy-Born rule can be expressed as:

$$\mathbf{r} = \mathbf{F}\mathbf{r}_0 \quad (5)$$

where \mathbf{F} is the deformation gradient tensor, \mathbf{r} and \mathbf{r}_0 are deformed and undeformed bond vectors, respectively.

In order to determine the equivalent energy density, which is related to the inter-atomic potential energy the corresponding concept to the strain energy density in the continuum mechanics should be considered. To this end, it is necessary to select a proper representative volume element (RVE) or representative cell by which the complete atomic structure could be reproduced. For carbon nanostructures, there are two RVE's, which are equivalent both in number of atoms and bonds located in the element and types of them. By considering the honeycomb structure in graphene sheets or carbon nanotubes, the preferred choice for the RVE is one of the hexagonal lattices. This cell is illustrated in Fig. (1). As can be seen, there are three types of bonds, A, B, and C with different orientations. It is noted that the two bonds with similar letters only contribute half of their potential energy to the RVE because they share the potential with the adjacent cell. Therefore, there are three complete bonds in the cell. The second choice for the RVE can be selected with rectangular shape as shown in Fig. (2).

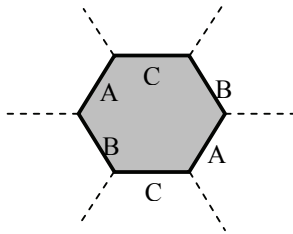


Figure 1: Hexagonal representative volume element for graphene sheet

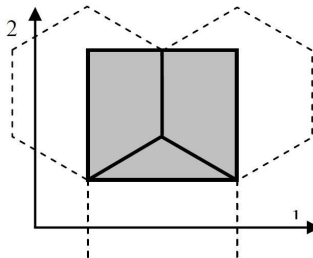


Figure 2: Rectangular representative volume element for graphene sheet

It is obvious that in the rectangular RVE there are also three complete bonds contributing to potential energy in the cell. It is note worthy that in the equivalent

continuum model, it is more realistic to use a rectangular shaped representative volume element. Therefore, the present RVE (Fig. 2) is an appropriate choice for energy homogenization. In addition, the rectangular RVE has an advantage in applying the chirality of the loading or the atomic structure to the formulation. When the orientation of the atomic structure changes, it is not necessary to choose another RVE, but required to rotate the rectangular RVE to meet the new orientation. This is done simply by applying the rotation tensors to the bond vectors. By computing the volume of the both RVEs, one can notice that the volumes are the same:

$$V_{RVE-Hex.} = 6 \times \frac{a}{2} \times \frac{a\sqrt{3}}{2} \times t_{eff} = \frac{3\sqrt{3}}{2} a^2 \times t_{eff} \quad (6)$$

$$V_{RVE-Rect.} = \frac{3a}{2} \times (a\sqrt{3}) \times t_{eff} = \frac{3\sqrt{3}}{2} a^2 \times t_{eff} \quad (7)$$

where a is the relaxed bond length, and t_{eff} is the effective thickness of the single layered graphene sheet.

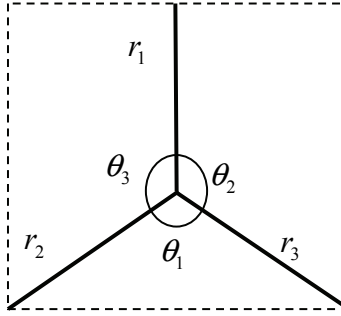


Figure 3: Numbering rule for bonds and angles in the rectangular RVE

Once we have selected the RVE, the potential energy in the RVE should be computed. Therefore, it is convenient to use a numbering rule for bonds and angles as shown in Fig. (3). The total potential energy in the RVE can be written as:

$$\phi_{RVE} = \sum_{i=1}^3 \phi(r_i) + 2 \sum_i \hat{\phi}(\theta_i) \quad (8)$$

where $\phi(r_i)$ and $\hat{\phi}(\theta_i)$ represent the modified Morse potential parts due to elongation of bond i and change in angle i , respectively. Dividing the energy by the RVE volume, the equivalent strain energy density in the RVE is calculated as follows:

$$\Phi_{RVE} = \frac{\phi_{RVE}}{V_{RVE}} \quad (9)$$

3.1 Kinematics

The Using the Cauchy-Born rule, Eq. (5), the bond length r_i can be written as a function of the deformation gradient tensor, \mathbf{F} , as follows:

$$r_i = \sqrt{\mathbf{r}_i \cdot \mathbf{r}_i} = \sqrt{\mathbf{F}\mathbf{r}_{0i} \cdot \mathbf{F}\mathbf{r}_{0i}} = \sqrt{\mathbf{r}_{0i} \cdot \mathbf{F}^T \mathbf{F} \mathbf{r}_{0i}} \quad i = 1, 2, 3 \quad (10)$$

where \mathbf{r}_i and \mathbf{r}_{0i} are the deformed and undeformed vector representation of bond i , respectively. According to the polar decomposition theorem in continuum mechanics, the deformation gradient tensor, \mathbf{F} , can uniquely be decomposed into a rotation tensor, \mathbf{R} , and symmetric tensors, \mathbf{U} and \mathbf{V} , in the form of:

$$\mathbf{F} = \mathbf{R}\mathbf{U} = \mathbf{V}\mathbf{R} \quad (11)$$

Substituting Eq. (11) into Eq. (10), we arrive at:

$$r_i = \sqrt{\mathbf{r}_{0i} \cdot \mathbf{F}^T \mathbf{F} \mathbf{r}_{0i}} = \sqrt{\mathbf{r}_{0i} \cdot \mathbf{U}^2 \mathbf{r}_{0i}} \quad i = 1, 2, 3 \quad (12)$$

The Green-Lagrange strain tensor, \mathbf{E} , is defined in terms of the right stretch tensor, \mathbf{U} , as follows:

$$\mathbf{E} = \frac{1}{2}(\mathbf{U}^2 - \mathbf{I}) \quad (13)$$

where \mathbf{I} is the identity tensor. Now we can substitute Eq. (13) into Eq. (12) to get the bond length in terms of the Green-Lagrange strain tensor:

$$r_i = \sqrt{\mathbf{r}_{0i} \cdot (\mathbf{I} + 2\mathbf{E}) \mathbf{r}_{0i}} = r_{0i} \sqrt{\mathbf{N}_i \cdot (2\mathbf{E} + \mathbf{I}) \mathbf{N}_i} \quad i = 1, 2, 3 \quad (14)$$

where r_{0i} is the undeformed length of bond i , and \mathbf{N}_i is the unit vector along the undeformed bond i defined as:

$$\mathbf{N}_i = \frac{\mathbf{r}_i}{r_i} \quad (15)$$

The cosine of the angle θ_i between bonds \mathbf{r}_j and \mathbf{r}_k can be written as:

$$\cos \theta_i = \frac{\mathbf{r}_j \cdot \mathbf{r}_k}{r_{0j} r_{0k}} = \frac{\mathbf{N}_j \cdot (2\mathbf{E} + \mathbf{I}) \mathbf{N}_k}{\sqrt{\mathbf{N}_j \cdot (2\mathbf{E} + \mathbf{I}) \mathbf{N}_j} \cdot \sqrt{\mathbf{N}_k \cdot (2\mathbf{E} + \mathbf{I}) \mathbf{N}_k}} \quad (16)$$

where the indices obey the permutation rule, i.e. $i = 1$ corresponds to $j = 2, k = 3$. Also, it is noted that since the undeformed length of all bonds are equal, we will suppress the index from the undeformed bond lengths and represent them by r_0 .

Considering the modified Morse potential (3) and using Eqs. (14) and (16), the terms in the RVE total potential energy (8) can be written as follows:

$$\begin{aligned}
 \phi(r_i) &= \phi_i = D_e \{ [1 - e^{-\beta r_0 (\sqrt{1+2\mathbf{N}_i \cdot \mathbf{E} \mathbf{N}_i} - 1)}]^2 - 1 \} \\
 \hat{\phi}(\theta_i) &= \hat{\phi}_i = \frac{1}{2} k_\theta \left(\arccos \frac{\mathbf{N}_j \cdot (2\mathbf{E} + \mathbf{I}) \mathbf{N}_k}{\sqrt{(\mathbf{N}_j \cdot (2\mathbf{E} + \mathbf{I}) \mathbf{N}_j) (\mathbf{N}_k \cdot (2\mathbf{E} + \mathbf{I}) \mathbf{N}_k)}} - \theta_0 \right)^2 \\
 &\quad \times [1 + k_{\text{sextile}} \left(\arccos \frac{\mathbf{N}_j \cdot (2\mathbf{E} + \mathbf{I}) \mathbf{N}_k}{\sqrt{(\mathbf{N}_j \cdot (2\mathbf{E} + \mathbf{I}) \mathbf{N}_j) (\mathbf{N}_k \cdot (2\mathbf{E} + \mathbf{I}) \mathbf{N}_k)}} - \theta_0 \right)^4]
 \end{aligned} \tag{17}$$

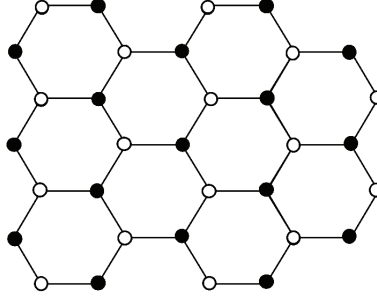


Figure 4: Sublattices in the non-centrosymmetric atomic structure

3.2 Cauchy-Born rule for non-centrosymmetric lattices

The Cauchy-Born rule in the form expressed in Eq. (5) is only applicable to the atomic structures that possess centrosymmetry. Clearly, the atomic structure of graphene sheets and carbon nanotubes do not meet this symmetry requirement. In other words, we can not use the relations in the previous section for carbon nanotubes. Klein (1999) showed that for non-centrosymmetric materials, inappropriate use of Cauchy-Born rule may lead to incorrect results.

For hexagonal lattice of graphene sheets and carbon nanotubes, we consider two sublattices which both possess centrosymmetry, and hence, Cauchy-Born rule can be used for either of them. These sublattices are recognized as black and white circles in Fig. (4). If the reference sublattice is the black one, which deforms under the action of the deformation gradient \mathbf{F} , the white sublattice besides being

subjected to \mathbf{F} , may also undergo a rigid-body translation expressed as $\mathbf{F}\boldsymbol{\xi}$. Thus, the deformed bonds in the RVE can be expressed as:

$$\mathbf{r}_i = \mathbf{F}\mathbf{r}_{0i} + \mathbf{F}\boldsymbol{\xi} = \mathbf{F}(\mathbf{r}_{0i} + \boldsymbol{\xi}) \quad (18)$$

The vector $\boldsymbol{\xi}$ related to the rigid-body translation, is determined by minimizing the strain energy density with respect to it. Form Eq. (18), the bond length can be obtained as:

$$\begin{aligned} r_i &= \sqrt{(\mathbf{r}_{0i} + \boldsymbol{\xi}) \cdot (\mathbf{I} + 2\mathbf{E})(\mathbf{r}_{0i} + \boldsymbol{\xi})} \\ &= r_{0i} \sqrt{(\mathbf{N}_i + \boldsymbol{\eta}) \cdot (2\mathbf{E} + \mathbf{I})(\mathbf{N}_i + \boldsymbol{\eta})} \quad i = 1, 2, 3 \end{aligned} \quad (19)$$

where the vector $\boldsymbol{\eta} = \boldsymbol{\xi}/r_0$.

The cosine of the bond angle can also be written as:

$$\begin{aligned} \cos \theta_i &= \frac{\mathbf{r}_j \cdot \mathbf{r}_k}{r_{0j} r_{0k}} \\ &= \frac{(\mathbf{N}_j + \boldsymbol{\eta}) \cdot (2\mathbf{E} + \mathbf{I})(\mathbf{N}_k + \boldsymbol{\eta})}{\sqrt{(\mathbf{N}_j + \boldsymbol{\eta}) \cdot (2\mathbf{E} + \mathbf{I})(\mathbf{N}_j + \boldsymbol{\eta})} \sqrt{(\mathbf{N}_k + \boldsymbol{\eta}) \cdot (2\mathbf{E} + \mathbf{I})(\mathbf{N}_k + \boldsymbol{\eta})}} \end{aligned} \quad (20)$$

Substituting Eqs. (19) and (20) into Eq. (8), the total potential energy of the RVE can be obtained:

$$\begin{aligned} \phi_i &= D_e \left\{ \left[1 - e^{-\beta r_0 (\sqrt{1 + 2(\mathbf{N}_i + \boldsymbol{\eta}) \cdot \mathbf{E}(\mathbf{N}_i + \boldsymbol{\eta})} - 1)} \right]^2 - 1 \right\} \\ \hat{\phi}_i &= \frac{1}{2} k_\theta \\ &\times \left(\arccos \frac{(\mathbf{N}_j + \boldsymbol{\eta}) \cdot (2\mathbf{E} + \mathbf{I})(\mathbf{N}_k + \boldsymbol{\eta})}{\sqrt{((\mathbf{N}_j + \boldsymbol{\eta}) \cdot (2\mathbf{E} + \mathbf{I})(\mathbf{N}_j + \boldsymbol{\eta})) ((\mathbf{N}_k + \boldsymbol{\eta}) \cdot (2\mathbf{E} + \mathbf{I})(\mathbf{N}_k + \boldsymbol{\eta}))}} - \theta_0 \right)^2 \\ &\times \left[1 + k_{\text{sextile}} \right. \\ &\times \left. \left(\arccos \frac{(\mathbf{N}_j + \boldsymbol{\eta}) \cdot (2\mathbf{E} + \mathbf{I})(\mathbf{N}_k + \boldsymbol{\eta})}{\sqrt{((\mathbf{N}_j + \boldsymbol{\eta}) \cdot (2\mathbf{E} + \mathbf{I})(\mathbf{N}_j + \boldsymbol{\eta})) ((\mathbf{N}_k + \boldsymbol{\eta}) \cdot (2\mathbf{E} + \mathbf{I})(\mathbf{N}_k + \boldsymbol{\eta}))}} - \theta_0 \right)^4 \right] \end{aligned} \quad (21)$$

As mentioned before, the vector $\boldsymbol{\eta}$ can be obtained by minimizing the potential energy:

$$\frac{\partial \phi_{RVE}}{\partial \boldsymbol{\eta}} = 0 \quad (22)$$

3.3 Constitutive model

Equation (21) represents a nonlinear strain energy density function, which is expressed as a function of some kinematical variables in the undeformed configuration. It is required to select suitable energy conjugate measures for strain and stress to derive the corresponding relation between them using the strain energy density function (21). Among the various measures for the strain and stress, the conjugate pair of the Green-Lagrange strain and the second Piola-Kirchhoff stress tensors are used. These Lagrangian measures are suitable for finite element formulation used for the analysis of large deformation problems. Therefore, differentiating Eq. (9) with respect to the Green-Lagrange strain tensor, we will find the second Piola-Kirchhoff stress tensor as follows:

$$\mathbf{S} = \frac{1}{V_{RVE}} \frac{d\phi_{RVE}}{d\mathbf{E}} = \frac{1}{V_{RVE}} \sum_i^3 \left(\frac{d\phi_i}{d\mathbf{E}} + 2 \frac{d\hat{\phi}_i}{d\mathbf{E}} \right) \quad (23)$$

where i runs from 1 to 3, for 3 bonds and angles. Considering Eqs. (3), the derivatives of the interatomic potential can be written as follows:

$$\begin{aligned} \frac{d\phi_i}{d\mathbf{E}} &= 2D_e(1 - e^{-\beta(r-r_0)}) \left(\beta \frac{dr}{d\mathbf{E}} e^{-\beta(r-r_0)} \right) \\ &= 2D_e\beta \frac{dr}{d\mathbf{E}} [e^{-\beta(r-r_0)} - e^{-2\beta(r-r_0)}] \end{aligned} \quad (24)$$

$$\begin{aligned} \frac{d\hat{\phi}_i}{d\mathbf{E}} &= k_\theta \frac{d\theta}{d\mathbf{E}} (\theta - \theta_0) [1 + k_s(\theta - \theta_0)^4] + \frac{1}{2} k_\theta (\theta - \theta_0)^2 [4k_s(\theta - \theta_0)^3 \frac{d\theta}{d\mathbf{E}}] \\ &= \frac{d\theta}{d\mathbf{E}} [k_\theta(\theta - \theta_0) + 3k_\theta k_s(\theta - \theta_0)^5] \\ &= k_\theta(\theta - \theta_0) \frac{d\theta}{d\mathbf{E}} [1 + 3k_s(\theta - \theta_0)^4] \end{aligned} \quad (25)$$

Using Eq. (19) we can calculate the derivative of the bond length with respect to the Green-Lagrange strain tensor:

$$\frac{dr_i}{d\mathbf{E}} = r_0 \frac{\left(\frac{d((\mathbf{N}_i + \eta) \cdot \mathbf{E}(\mathbf{N}_i + \eta))}{d\mathbf{E}} \right)}{\sqrt{1 + 2(\mathbf{N}_i + \eta) \cdot \mathbf{E}(\mathbf{N}_i + \eta)}} \quad (26)$$

where the components of the tensor $\frac{d((\mathbf{N}_i+\boldsymbol{\eta})\cdot\mathbf{E}(\mathbf{N}_i+\boldsymbol{\eta}))}{d\mathbf{E}}$ can be written as follows:

$$\begin{aligned} \left[\frac{d((\mathbf{N}_i+\boldsymbol{\eta})\cdot\mathbf{E}(\mathbf{N}_i+\boldsymbol{\eta}))}{d\mathbf{E}} \right]_{pq} &= \frac{d(N_{ip}+\eta_p)E_{pr}(N_{ir}+\eta_r)}{dE_{pq}} \\ &= (N_{ip}+\eta_p) \frac{dE_{pr}}{dE_{pq}} (N_{ir}+\eta_r) \\ &= (N_{ip}+\eta_p) \frac{d(E_{pq}\delta_{qr})}{dE_{pq}} (N_{ir}+\eta_r) \\ &= (N_{ip}+\eta_p)\delta_{qr}(N_{ir}+\eta_r) \\ &= (N_{ip}+\eta_p)(N_{iq}+\eta_q) \end{aligned} \quad (27)$$

Eq. (27) can be written in the form of dyadic (tensorial) product:

$$\frac{d((\mathbf{N}_i+\boldsymbol{\eta})\cdot\mathbf{E}(\mathbf{N}_i+\boldsymbol{\eta}))}{d\mathbf{E}} = (\mathbf{N}_i+\boldsymbol{\eta}) \otimes (\mathbf{N}_i+\boldsymbol{\eta}) \quad (28)$$

Substituting Eq. (28) into (26), the derivative of r_i with respect to \mathbf{E} can be written as:

$$\frac{dr_i}{d\mathbf{E}} = r_0 \frac{(\mathbf{N}_i+\boldsymbol{\eta}) \otimes (\mathbf{N}_i+\boldsymbol{\eta})}{\sqrt{1+2(\mathbf{N}_i+\boldsymbol{\eta})\cdot\mathbf{E}(\mathbf{N}_i+\boldsymbol{\eta})}} \quad (29)$$

The bending or bond angle variation part of the modified Morse potential contains the angles θ_1 , θ_2 , and θ_3 . In order to differentiate the angles with respect to the Green-Lagrange strain tensor, considering Eq. (20), and using the chain rule

$$\begin{aligned} u &= \cos \theta_i \\ &= \frac{(\mathbf{N}_j+\boldsymbol{\eta})\cdot(2\mathbf{E}+\mathbf{I})\cdot(\mathbf{N}_k+\boldsymbol{\eta})}{\sqrt{(\mathbf{N}_j+\boldsymbol{\eta})\cdot(2\mathbf{E}+\mathbf{I})\cdot(\mathbf{N}_j+\boldsymbol{\eta})}\cdot\sqrt{(\mathbf{N}_k+\boldsymbol{\eta})\cdot(2\mathbf{E}+\mathbf{I})\cdot(\mathbf{N}_k+\boldsymbol{\eta})}} \end{aligned} \quad (30)$$

$$(\arccos u)' = -\frac{u'}{\sqrt{1-u^2}} \quad (31)$$

we obtain

$$\begin{aligned} u' &= \frac{d \cos \theta_i}{d\mathbf{E}} = \\ &= \frac{2((\mathbf{N}_j+\boldsymbol{\eta}) \otimes (\mathbf{N}_k+\boldsymbol{\eta})) \left[\begin{array}{c} (1+2(\mathbf{N}_j+\boldsymbol{\eta})\cdot\mathbf{E}(\mathbf{N}_j+\boldsymbol{\eta})) \\ \times (1+2(\mathbf{N}_k+\boldsymbol{\eta})\cdot\mathbf{E}(\mathbf{N}_k+\boldsymbol{\eta})) \end{array} \right]}{[(1+2(\mathbf{N}_j+\boldsymbol{\eta})\cdot\mathbf{E}(\mathbf{N}_j+\boldsymbol{\eta}))(1+2(\mathbf{N}_k+\boldsymbol{\eta})\cdot\mathbf{E}(\mathbf{N}_k+\boldsymbol{\eta}))]^{\frac{3}{2}}} \\ &\quad - \frac{\left\{ \begin{array}{c} ((\mathbf{N}_j+\boldsymbol{\eta})\cdot(2\mathbf{E}+\mathbf{I})\cdot(\mathbf{N}_k+\boldsymbol{\eta})) \times \\ \left[\begin{array}{c} (\mathbf{N}_j+\boldsymbol{\eta}) \otimes (\mathbf{N}_j+\boldsymbol{\eta}) (1+2(\mathbf{N}_k+\boldsymbol{\eta})\cdot\mathbf{E}(\mathbf{N}_k+\boldsymbol{\eta})) \\ + (\mathbf{N}_k+\boldsymbol{\eta}) \otimes (\mathbf{N}_k+\boldsymbol{\eta}) (1+2(\mathbf{N}_j+\boldsymbol{\eta})\cdot\mathbf{E}(\mathbf{N}_j+\boldsymbol{\eta})) \end{array} \right] \end{array} \right\}}{[(1+2(\mathbf{N}_j+\boldsymbol{\eta})\cdot\mathbf{E}(\mathbf{N}_j+\boldsymbol{\eta}))(1+2(\mathbf{N}_k+\boldsymbol{\eta})\cdot\mathbf{E}(\mathbf{N}_k+\boldsymbol{\eta}))]^{\frac{3}{2}}} \end{aligned} \quad (32)$$

The derivative of the angle with respect to Green-Lagrange strain tensor $\frac{d\theta_i}{d\mathbf{E}}$ can be obtained by substituting Eqs. (32) and (30) into Eq. (31). By substituting the derivatives into Eq. (23), we can write the equation for the bond elongation and bond angle variation parts of the constitutive equation as follows:

$$\frac{d\phi_i}{d\mathbf{E}} = 2D_e\beta r_0 \frac{(\mathbf{N}_i + \boldsymbol{\eta}) \otimes (\mathbf{N}_i + \boldsymbol{\eta})}{\sqrt{1 + 2(\mathbf{N}_i + \boldsymbol{\eta}) \cdot \mathbf{E}(\mathbf{N}_i + \boldsymbol{\eta})}} \times [e^{-\beta r_0(\sqrt{1+2(\mathbf{N}_i+\boldsymbol{\eta}) \cdot \mathbf{E}(\mathbf{N}_i+\boldsymbol{\eta})}-1)} - e^{-2\beta r_0(\sqrt{1+2(\mathbf{N}_i+\boldsymbol{\eta}) \cdot \mathbf{E}(\mathbf{N}_i+\boldsymbol{\eta})}-1)}] \quad (33)$$

$$\begin{aligned} \frac{d\hat{\phi}_i}{d\mathbf{E}} &= k_\theta \frac{d\theta_i}{d\mathbf{E}} \\ &\times \left(\arccos \frac{(\mathbf{N}_j + \boldsymbol{\eta}) \cdot (2\mathbf{E} + \mathbf{I}) \cdot (\mathbf{N}_k + \boldsymbol{\eta})}{\left[\begin{array}{l} \sqrt{(\mathbf{N}_j + \boldsymbol{\eta}) \cdot (2\mathbf{E} + \mathbf{I}) \cdot (\mathbf{N}_j + \boldsymbol{\eta})} \\ \times \sqrt{(\mathbf{N}_k + \boldsymbol{\eta}) \cdot (2\mathbf{E} + \mathbf{I}) \cdot (\mathbf{N}_k + \boldsymbol{\eta})} \end{array} \right]} - \theta_0 \right) \\ &\times [1 + 3k_s \left(\arccos \frac{(\mathbf{N}_j + \boldsymbol{\eta}) \cdot (2\mathbf{E} + \mathbf{I}) \cdot (\mathbf{N}_k + \boldsymbol{\eta})}{\left[\begin{array}{l} \sqrt{(\mathbf{N}_j + \boldsymbol{\eta}) \cdot (2\mathbf{E} + \mathbf{I}) \cdot (\mathbf{N}_j + \boldsymbol{\eta})} \\ \times \sqrt{(\mathbf{N}_k + \boldsymbol{\eta}) \cdot (2\mathbf{E} + \mathbf{I}) \cdot (\mathbf{N}_k + \boldsymbol{\eta})} \end{array} \right]} - \theta_0 \right)^4] \end{aligned} \quad (34)$$

Substituting Eq. (34) into Eq. (23), the second Piola-Kirchhoff stress tensor can be computed in terms of the Green-Lagrange strain tensor.

The following remarks can be made considering the nonlinear constitutive model for carbon nanostructures derived in this section:

There were no simplification in the interatomic potential used in the formulation.

Because we have used the Lagrangian description for the formulation, the proposed constitutive model can successfully be applied in the large deformation problems.

The orientation of the atomic structure in the undeformed or reference configuration which is called chirality, is a built-in characteristic of the constitutive model, therefore the effect of the chirality on the mechanical behavior of the atomic structure can be easily modeled by switching the chirality parameter.

The homogenization technique, which is used to homogenize the discrete atomic potential to a uniform continuous one, is the Cauchy-Born rule. The standard Cauchy-Born rule is suitable for flat structures such as graphene sheet and can be applied to flat structures without any extra work. For curved structures such as carbon nanotubes, some modification is necessary to successfully homogenize the deformation field. Arroyo and Belytschko presented the exponential Born rule which is formulated using the exponential map of tangents of manifolds on them.

It is noted that although the formulation is expressed in terms of second Piola-Kirchhoff stress tensor \mathbf{S} , it can be converted to the Cauchy stress tensor with the

following relation:

$$\boldsymbol{\sigma} = \frac{1}{J} \mathbf{F} \mathbf{S} \mathbf{F}^T \quad (35)$$

where $\boldsymbol{\sigma}$ is Cauchy stress tensor, J is the Jacobian of the deformation (determinant of the deformation gradient, \mathbf{F}).

3.4 Elasticity Tensor

In order to derive the elasticity tensor based on the constitutive equation developed in the previous section, the second derivative of the potential energy (strain energy density) should be determined. Considering Eq. (24) and differentiating it with respect to \mathbf{E} we arrive at:

$$\begin{aligned} \frac{d^2 \phi_i}{d\mathbf{E}d\mathbf{E}} = 2D_e \beta \frac{d^2 r}{d\mathbf{E}d\mathbf{E}} & \left(e^{-\beta(r-r_0)} - e^{-2\beta(r-r_0)} \right) \\ & + 2D_e \beta \frac{dr}{d\mathbf{E}} \otimes \left(-\beta \frac{dr}{d\mathbf{E}} e^{-\beta(r-r_0)} + 2\beta \frac{dr}{d\mathbf{E}} e^{-2\beta(r-r_0)} \right) \end{aligned} \quad (36)$$

Also, differentiating Eq. (25) we obtain:

$$\begin{aligned} \frac{d^2 \hat{\phi}_i}{d\mathbf{E}d\mathbf{E}} = \frac{d^2 \theta}{d\mathbf{E}d\mathbf{E}} & [k_\theta (\theta - \theta_0) + 3k_\theta k_s (\theta - \theta_0)^5] \\ & + \frac{d\theta}{d\mathbf{E}} \otimes \left[k_\theta \frac{d\theta}{d\mathbf{E}} + 15k_\theta k_s \frac{d\theta}{d\mathbf{E}} (\theta - \theta_0)^4 \right] \end{aligned} \quad (37)$$

where the term $\frac{d^2 r}{d\mathbf{E}d\mathbf{E}}$ can be calculated considering Eq. (29):

$$\frac{d^2 r}{d\mathbf{E}d\mathbf{E}} = -r_0 \frac{((\mathbf{N} + \boldsymbol{\eta}) \otimes (\mathbf{N} + \boldsymbol{\eta})) \otimes ((\mathbf{N} + \boldsymbol{\eta}) \otimes (\mathbf{N} + \boldsymbol{\eta}))}{(1 + 2(\mathbf{N} + \boldsymbol{\eta}) \cdot \mathbf{E}(\mathbf{N} + \boldsymbol{\eta}))^{3/2}} \quad (38)$$

It is noted that in Eqs. (36) and (37), $\frac{d^2 r}{d\mathbf{E}d\mathbf{E}}$ and $\frac{d^2 \theta}{d\mathbf{E}d\mathbf{E}}$ are fourth-order tensors, and $\frac{dr}{d\mathbf{E}}$ and $\frac{d\theta}{d\mathbf{E}}$ are second order tensors. Therefore, the elasticity tensor is obtained by using Eqs. (36) and (37) represent when they summed over the RVE.

3.5 Effects of the curvature

The curvature of carbon nanotube is the most important difference with the flat atomic structure of the graphene sheet. Considering a (n, n) armchair nanotube, the RVE is no longer planar due to the curvature of the nanotube and the angles between

adjacent bonds are different from those in the graphene sheet. Considering the non-planar RVE in the Fig. (5), the following relations are governing the angles:

$$\theta_1 = \theta_2 = \pi - \arccos\left(\frac{1}{2} \cos \frac{\pi}{2n}\right) \quad \theta_3 = \frac{2\pi}{3} \quad \beta_1 = \beta_2 = 0 \quad \beta_3 = \frac{\pi}{2n} \quad (39)$$

where, θ_1 , θ_2 and θ_3 are the angles between bonds and β_1 , β_2 and β_3 are the out-of-plane angles as defined in Fig. (5).

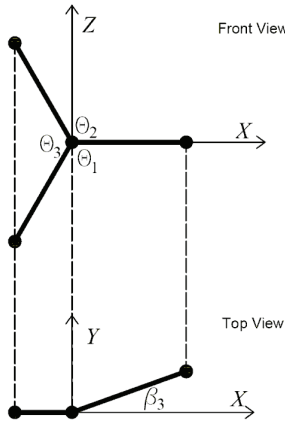


Figure 5: The non-planar RVE of an armchair nanotube

Considering the non-planar RVE of the armchair nanotube, the unit vectors aligned in the direction of the undeformed bond vectors \mathbf{r}_1 , \mathbf{r}_2 , and \mathbf{r}_3 can be written as:

$$\begin{aligned} \mathbf{N}_1 &= \left\{ -\cos\left(\frac{\pi}{3}\right); 0; \sin\left(\frac{\pi}{3}\right) \right\} \\ \mathbf{N}_2 &= \left\{ -\cos\left(\frac{\pi}{3}\right); 0; -\sin\left(\frac{\pi}{3}\right) \right\} \\ \mathbf{N}_3 &= \left\{ \cos\left(\frac{\pi}{2n}\right); \sin\left(\frac{\pi}{2n}\right); 0 \right\} \end{aligned} \quad (40)$$

The unit vectors are functions of n , the Hamada index of the armchair nanotubes, i.e. n in the (n, n) nanotube. The following remarks can be made on the effects of the curvature on the constitutive equation:

The curvature of the nanotube modeled by a non-planar RVE affects the undeformed (reference) configuration of the atomic bonds and angles. In order to apply

the curvature effects in the armchair nanotubes, modified unit vectors should be used in the constitutive model derived in the previous section.

The radius of the nanotube appears implicitly by the Hamada index of the nanotube. In the application, one can directly specify the Hamada index or the diameter of the nanotube (diameter of the nanotube can be obtained knowing the Hamada index).

4 Results and Discussion

Applying Eq. (40) into the constitutive model derived in the previous section, we have studied the elastic response of the graphene sheets and armchair carbon nanotubes in uniaxial extension.

4.1 Tension of the Graphene Sheet

In this section, we do some simulations to show the behavior of the graphene sheet and carbon nanotube. We start with stretching the graphene sheet in a fixed direction and study the stress-stretch behavior of it. To this end, we apply the unidirectional form of the deformation gradient tensor, Eq. (41), to the constitutive equation and obtain the stress tensor.

$$\mathbf{F} = U\mathbf{e}_1 \otimes \mathbf{e}_1 + \mathbf{e}_2 \otimes \mathbf{e}_2 + \mathbf{e}_3 \otimes \mathbf{e}_3 \quad (41)$$

Fig. (6) shows Cauchy stress versus stretch for a single layered graphene sheet under uniaxial tension. As can be seen from the figure, the stress-stretch relation is a nonlinear curve that has a maximum, and afterward decays to zero. This relation between stress and stretch is obtained merely from the constitutive model without introducing any failure or damage function. Thus, using the presented constitutive model, bond separations and crack propagations can be simulated with no other special considerations.

4.2 Elastic moduli of carbon nanotubes

Elastic properties of carbon nanotubes can be calculated from the constitutive model we obtained in the previous section. Fig. (7) shows the variation of Young's modulus with diameter of the nanotube. Young's modulus increases with increasing diameter, and the curve flattens for large diameters of nanotube. The value of Young's modulus approaches to that of graphene sheet for large values of nanotube diameter in which the curvature effect diminishes; i.e. 1.096 TPa. The same behavior is observed for shear modulus of nanotubes, illustrated in Fig. (8). The shear modulus of nanotube reaches that of graphene sheet for large values of diameter; i.e. 423 GPa.

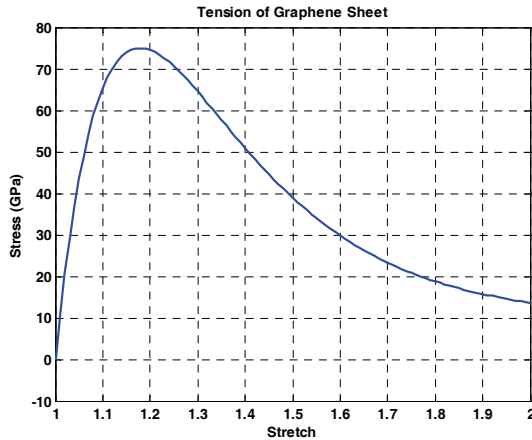


Figure 6: Stress-Stretch curve for a single layered graphene sheet under tension

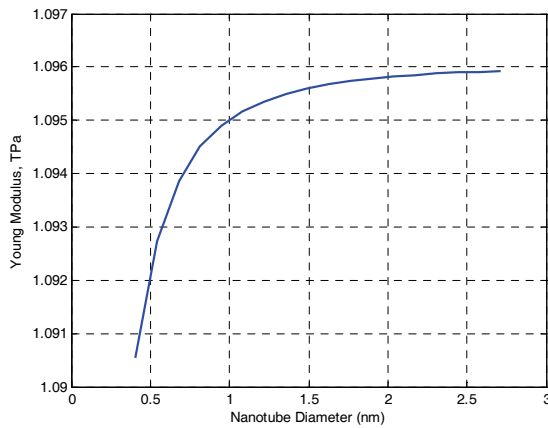


Figure 7: Variation of Young's modulus with nanotube diameter

It is concluded from Figs. (7) and (8) that for small values of nanotube diameter, e.g. smaller than 1 nm, there is a strong dependency of the Young's and shear moduli of nanotube on its diameter. However, for larger diameters, this dependency becomes very weak. This is due to the fact that for smaller diameters, the curvature of nanotube plays an important role in distorting the C-C bond; and when the diameter increases, the curvature becomes very small and the atomic structure of nanotube approaches to that of graphene sheet.

Fig. (9) shows the results of the present model in comparison with the existing results. As can be seen, the results obtained from the present model are in a good agreement with those obtained using other approaches. It is noted that the results reported here from the literature are obtained using direct modeling of CNT atomic structure and detailed modeling of atomic bonds. On the other hand, our results are solely obtained from the constitutive model without the need for using detailed atomic structure of the nanotubes.

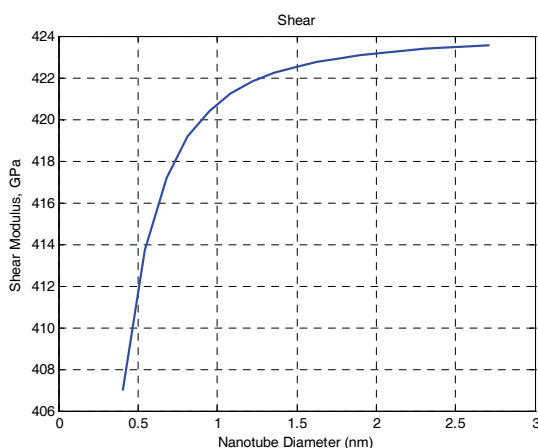


Figure 8: Variation of shear modulus with nanotube diameter

Wu *et al.* (2006) obtained Young's modulus of graphene sheet based on an energy-equivalent model to be 1.06 TPa. Popov *et al.* (2000) calculated graphite Young's modulus to be about 1.0 TPa. Xiao *et al.* (2005) gave graphite Young's modulus of 1.13 TPa using an analytical molecular structure mechanics model. Furthermore, our predicted results are comparable to those obtained from experiments. For example, Krishnan *et al.* (1998) reported an average Young's modulus of 1.3 TPa from measured amplitudes of 27 SWCNTs. Yu *et al.* (2004) got Young's modulus ranging from 0.32 to 1.47 TPa for SWCNT and from 0.27 to 0.95 TPa for MWCNT by performing direct tensile loading tests. Wong *et al.* (1997) obtained Young's modulus of MWCNT of 1.287 TPa by using a cantilever beam model to simulate the deflection of MWCNT.

The shear modulus of carbon nanotube obtained using the present constitutive modeling in comparison with the existing results is shown in Fig. (10). The torsion response of nanotubes has received much less attention than the tensile behavior of nanotubes. Some theoretical studies have been conducted by Xiao *et al.* (2005),

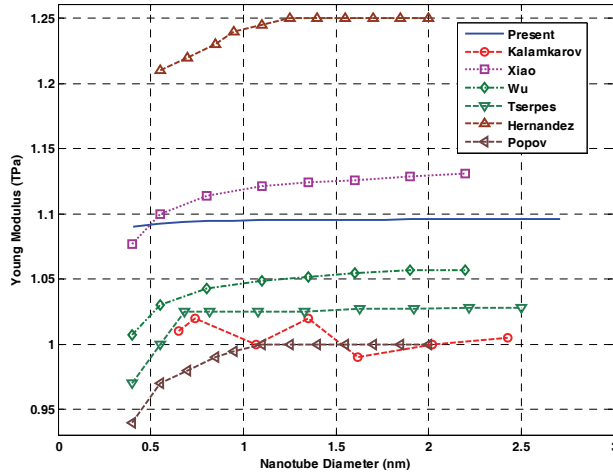


Figure 9: Comparison of Young's modulus between present model and existing results

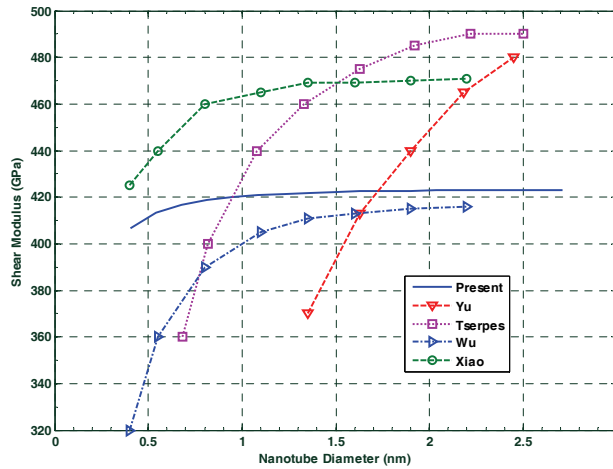


Figure 10: Comparison of shear modulus between present model and existing results

Popov *et al.* (2000) whose results are compared with our results in Fig. (10).

5 Conclusions

A multiscale nonlinear tensorial constitutive model has been presented based on the modified Morse potential for the analysis of carbon nanostructures. Lagrangian description is used to express the stress-strain relation in this constitutive model. The second Piola-Kirchhoff stress tensor and the Green-Lagrange strain tensor are selected as stress and strain measures, respectively. No simplification were made on the interatomic potential function and thus the constitutive model contains all the atomic data provided by the interatomic potential function. For the case of armchair carbon nanotubes, the effects of the curvature are considered in the constitutive model using a non-planar RVE. The continuum-based constitutive model presented here includes the effect of the curvature of the nanotube as a built-in property. Using the presented constitutive model, the effects of the nanotube diameter on the elastic response has been studied. The results obtained for the elastic properties of nanotubes with varying diameters are in a good agreement with the exact modeling of bonds and atoms using methods such as molecular mechanics and dynamics. In addition, it has been shown that when the diameter of the nanotube becomes smaller than a certain value for each loading case, the curvature of the nanotube plays an important role in the elastic behavior of the nanotube.

Therefore, there is a good potential for using the presented constitutive model in a finite element formulation in which the nanotube is modeled using continuum shell elements. This way, complicated behavior of the nanotube, i.e. buckling, wrinkling, etc., could be analyzed by the finite element method using the presented constitutive model.

References

- Arroyo, M. ; Belytschko, T.** (2002): An atomistic-based finite deformation membrane for single layer crystalline films, *J. Mech. Phys. Solid*, vol. 50, pp. 1941-1977.
- Behfar, K.; Naghdabadi, R.** (2005): Nanoscale vibrational analysis of a multi-layered graphene, *Compos. Sci. Tech.* vol. 65, pp. 1159-1164.
- Behfar, K.; Naghdabadi, R.** (2006): Nanoscale modeling of an embedded multi-shell fullerene and its application to vibrational analysis, *Int. J. Eng. Sci.*, vol. 44, pp. 1156–1163.
- Belytschko, T.; Xiao, S. P.** (2003): Coupling Methods for Continuum Model with Molecular Model, *Int J. Multiscale Comput. Eng.*, vol. 1, pp. 115-126.

- Belytschko, T.; Xiao, S. P.; Schatz, G. C.; Ruoff, R.** (2002): Atomistic simulations of nanotube fracture, *Phys. Rev. B.*, vol. 65 pp. 235430/1-8,.
- Born, M.; Oppenheimer, J. R.** (1927): Zur quantentheorie, (*Ann. Phys.*, Leipzig, vol. 84, pp. 457) (cited from Park, D.; Introduction to the Quantum Theory, McGraw-Hill, New York, 1992)
- Brenner, D.** (1990) Empirical potential for hydrocarbons for use in simulating chemical vapor deposition of diamond films. *Phys. Rev. B*, vol. 42, pp. 9458–9471.
- Chakrabarty, A.; Cagin, T.** (2008): Computational studies on mechanical and thermal properties of carbon nanotube based nanostructures. *CMC: Computers, Materials & Continua*, vol.7, no.3, pp.167-189.
- Chung, P. W.; Namburu, R. R.** (2003): On a formulation for a Multiscale atomistic-continuum homogenization method, *Int. J. Solids & Struct.*, vol. 40, pp. 2563–2588.
- Deymier, P. A.; Vasseur, J. O.** (2002): Concurrent multiscale model of an atomic crystal coupled with elastic continua, *Phys. Rev. B*, vol. 66, pp. 134106.
- Ericksen, J. L.** (1984): Phase Transformations and Material Instabilities in Solids ed. M. Gurtin (Academic, NewYork,) pp. 61–77.
- Ghoniem, N. M.; Busso, E. P.; Kioussis, N.; Huang, H.** (2003): Multiscale modelling of nanomechanics and micromechanics: an overview, *Phil. Mag.* vol. 83, pp. 3475–3528.
- Gosh, S. K.** (2003): Density functional theory and multiscale materials modeling, *Bull. Mater. Sci.*, vol. 26 pp. 3–12.
- He, L. H.; Lim, C. W.; Wu, B. S.** (2004): A continuum model for size-dependent deformation of elastic films of nano-scale thickness, *Int. J. Solids & Struct.*, vol. 41, pp. 847-857.
- Hernandez, E.; Goze, C.; Bernier, P.; Rubio, A.** (1999): Elastic properties of single-wall nanotubes, *Appl. Phys. A*, vol. 68, pp. 287–292.
- Horstemeyer, M. F.; Baskes, M. I.; Prantil, V. C.; Philliber, J.; Vonderheide, S.** (2003): A multiscale analysis of fixed-end simple shear using molecular dynamics, crystal plasticity, and a macroscopic internal state variable theory, *Modelling Simul. Mater. Sci. Eng.* vol. 11, pp. 265–286.
- Hou, T. Y.; Wu, X. H.** (1997): A Multiscale Finite Element Method for Elliptic Problems in Composite Materials and Porous Media, *J. Comput. Phys.* vol. 134, pp. 169–189.
- Kalamkarov, A. L.; Georgiades, A. V.; Rokkam, S. K.; Veedu, V. P.; Ghasemi-Nejhad, M. N.** (2006): Analytical and numerical techniques to predict carbon nan-

otubes properties, *Int. J. Solids & Struct.* vol. 43 pp. 6832-6854.

Kaminski, M. (2005): Multiscale homogenization of n-component composites with semi-elliptical random interface defects, *Int. J. Solids & Struct.* vol. 42, pp. 3571–3590.

Karakasidis, T. E.; Charitidis, C. A. (2006): Multiscale modeling in nanomaterials science, *Mater. Sci. Eng. C*, doi:10.1016/j.msec.2006.06.029.

Klein, P. A. (1999): A virtual internal bond approach to modeling crack nucleation and growth. Ph.D. dissertation, Stanford University, Palo Alto, CA 94305.

Krishnan, A., Dujardin, E., Ebbesen, T.W., Yianilos, P.N., Treacy, M.M.J., (1998): Young's modulus of single-walled nanotubes. *Physical Review B*, vol. 58, pp. 14013–14019.

Li, C.; Chou, T. W. (2006): Multiscale modeling of compressive behavior of carbon nanotube/polymer composites, *Compos. Sci. Tech.* vol. 66, pp. 2409-2414.

Li, S.; Gupta, A.; Liu, X.; Mahyari, M. (2004): Variational eigenstrain multiscale finite element method, *Comput. Methods Appl. Mech. Engrg.* vol. 193, pp. 1803–1824.

Lurie, S. A.; Belov, P. A.; Tuchkov, N. P. (2005): The application of the multiscale models for description of the dispersed composites, *Composites: Part A*, vol. 36, pp. 145–152.

Maiti, A. (2006): Multiscale modeling with carbon nanotubes, *Microelectron. J.* doi:10.1016/j.mejo.2006.06.003

Morse, P. M. (1929) Diatomic molecules according to the wave mechanics. II. Vibrational level. *Phys. Rev.* pp. 34-57.

Odegard, G. M.; Frankland, S. J. V.; Herzog, M. N.; Gates, T. S.; Fay C. C. (2004): Constitutive Modeling of Crosslinked Nanotube Materials, in *Proc. 45th AIAA/ASME/ASCE/AHS/ASC Structures, Structural Dynamics & Materials Conference*, April 2004, (Palm Springs, California, 2004).

Odegard, G. M.; Gates, T. S. (2002) Equivalent-Continuum Modeling With Application to Carbon Nanotubes, Langley Research Center, Report: *NAS 1.15:211454; NASA/TM-2002-211454,L-18152*, 30p.

Peng, Y. J.; Zhang, L. Y.; Jin, Q. H.; Li, B. H.; Ding, D. T. (2006): Ab initio studies of elastic properties and electronic structures of C and BN nanotubes, *Physica E*, vol. 33, pp. 155–159.

Popov, V. N.; Van Doren, V. E.; Balkanski, M. (2000): Elastic properties of singlewalled carbon nanotubes, *Phys Rev B*, vol. 61, pp. 3078–3084.

Qian, D.; Wagner, G. J.; Liu, W. K. (2004): A multiscale projection method for

the analysis of carbon nanotubes, *Comput. Methods Appl. Mech. Engrg.* Vol. 193, pp. 1603–1632.

Sheng, N.; Boyce, M. C.; Parks, D. M.; Rutledge, G. C.; Abes, J. I.; Cohen, R. E. (2004): Multiscale micromechanical modeling of polymer/clay nanocomposites and the effective clay particle, *Polymer*, vol. 45, pp. 487–506.

Smaoui, S.; Ben Hamida A.; Djeran-Maigre, I.; Dumontet, H. (2006): Micro-macro approaches coupled to an iterative process for nonlinear porous media. *CMC: Computers, Materials & Continua*, Vol. 4, No. 3, pp. 153–162.

Sohi, A. N.; Naghdabadi, R. (2007a): Torsional buckling of carbon nanopeapods, *Carbon*, vol. 45, pp. 952–957.

Sohi, A. N.; Naghdabadi, R. (2007b): Stability of C60-peapods under hydrostatic pressure, *Acta Mater.*, doi:10.1016/j.actamat.2007.06.007.

Tadmor, E.; Smith, G.; Bernstein, N.; Kaxiras, E. (1999): Mixed finite element and atomistic formulation for complex crystals. *Phys. Rev. B*, vol. 59, pp. 235–245.

Tserpes, K. I.; Papanikos, P. (2005): Finite element modeling of single-walled carbon nanotubes, *Composites: Part B*, vol. 36, pp. 468–477.

Wagner, G. J.; Liu, W. K. (2003): Coupling of Atomistic and Continuum Simulations using a Bridging Scale Decomposition, *J. Comput. Phys.*, vol. 190, pp. 249–274.

Weinan, E.; Bjorn, E.; Zhongyi, H. (2003): Heterogeneous multiscale method: A general methodology for multiscale modeling, *Phys. Rev. B*, vol. 67, pp. 092101.

Wong, E., Sheehan, P.E., Lieber, C.M., (1997): Nanobeam mechanics: elasticity, strength, and toughness of nanorod and nanotubes. *Science*, vol. 277, pp. 1971–1975.

Wu, Y.; Zhang, X.; Leung, A. Y. T.; Zhong, W. (2006): An energy-equivalent model on studying the mechanical properties of single-walled carbon nanotubes, *Thin-Walled Structures*, vol. 44, pp. 667–676.

Wuite, J.; Adali, S. (2005): Deflection and stress behaviour of nanocomposite reinforced beams using a multiscale analysis, *Compos. Struct.* vol. 71, pp. 388–396.

Xiao, J. R.; Gama, B. A.; Gillespie Jr, J. W. (2005): An analytical molecular structural mechanics model for the mechanical properties of carbon nanotubes. *Int. J. Solids Struct.*, vol. 42, pp. 3075–3092.

Xie, G. Q.; Long, S. Y. (2006): Elastic vibration behaviors of carbon nanotubes based on micropolar mechanics. *CMC: Computers, Materials & Continua*, Vol. 4, No. 1, pp. 11–20.

Xie, G. Q.; Han, X.; Long, S. Y. (2007): Characteristic of waves in a multi-walled carbon nanotube. *CMC: Computers, Materials & Continua*, vol.6, no.1, pp.1-11

Yu, W.; Xi, W. X.; Xianggui, N. (2004) Atomistic simulation of the torsion deformation of carbon nanotubes, *Modelling Simul. Mater. Sci. Eng.* vol. 12, pp. 1099–1107.

Zbib, H. M.; Rubia, T. D. (2002): A multiscale model of plasticity, *Int. J. Plast.* vol. 18, pp. 1133–1163.

Zhang, P.; Huang, Y. ; Geubelle, P. H.; Klein, P. A.; Hwang, K. C. (2002): The elastic modulus of single-wall carbon nanotubes, a continuum analysis incorporating interatomic potentials, *Int. J. Solids & Struct.*, vol. 39, pp. 3893-3906.